VIII International Conference on Computational Plasticity
COMPLAS VIII
E. Oñate and D.R.J. Owen (Eds)

A MICRO-MACRO APPROACH FOR CEMENT-BASED CONSTRUCTION MATERIALS

Michael Hain, Peter Wriggers

Institute of Mechanics and Computational Mechanics
University of Hannover
Appelstr. 9A, D-30167 Hannover, Germany
e-mail: hain@ibnm.uni-hannover.de, web page: http://www.ibnm.uni-hannover.de

Key words: hardened cement paste, micro-macro approach, homogenization, parameter identification.

Summary. *For a better understanding of material phenomena, it is necessary to take a deeper look into the microstructure of the considered material. In this contribution we focus on hardened cement paste with the goal to determine the effective material properties. Based on a three-dimensional computer-tomography, a finite-element mesh is constructed at the micrometer length scale. To obtain the desired inelastic material parameters, one has to solve an inverse problem. Once the material parameters at the microscopic length scale are identified, homogenized material properties are obtained.*

1 Introduction

For a better understanding of material phenomena, a multi-scale model for hardened cement paste is developed. The scale of the superior system is denoted macro-scale, the underlying microscopic system micro-scale[4,7]. The geometry at the micro-scale is obtained from a three-dimensional computer-tomography (CT) at a resolution of $1\mu m$. In **Figure 1**, a cut through of such a three dimensional CT-scan with an edge length of $1008\mu m$ is shown. The unhydrated part is black and the hydrated part is middle gray colored. One can see the accumulation of pores, which are marked in light gray. The volume fraction of the hydrated part is approximately 84 $vol\%$.

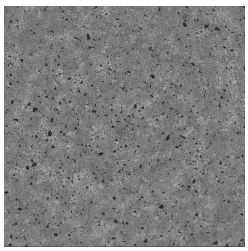

Figure 1: Raw data.

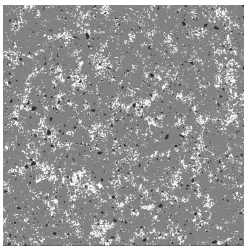

Figure 2: Segmented data.

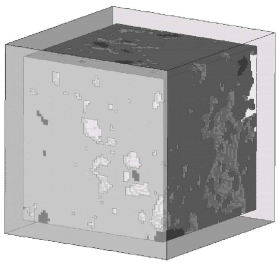

Figure 3: RVE.

In order to eliminate noise, a median filter has to be applied. Then, unhydrated cement, hydration products and porosity can be distinguished, making use of the theory from Powers and coworkers[5,6]. In **Figure 2**, the filtered data are shown, which are obtained from the raw data, see **Figure 1**. For computations, representative volume elements (RVEs) with an edge length of $64\mu m$ (64^3 finite-elements) are used. The RVEs are embedded in a matrix of average stiffness, to avoid problems at the boundary (see **Figure 3**). Results on the micro-structural level are obtained using the finite-element method. Accordingly, each RVE contains 800 000 DOFs.

2 Constitutive equations for the RVE

Material properties for the elastic part can directly be taken from the literature[1,2,3]. The pores are described with a linear-elastic material of negligible stiffness to avoid numerical problems.

phase	$E\left[\frac{N}{mm^2}\right]$	$\nu[-]$
unhydrated phase	$\approx$ 132 700	0.30
hydrated phase	19 500	0.21
pores	1	0.00

Table 1: Elastic properties phases.

For the hydrated phase, a visco-plastic model of PERZYNA-type combined with an isotropic damage model is chosen. The stress-strain relation for the damage is given by $\boldsymbol{\sigma} = (1-D)\mathbb{C} : \boldsymbol{\epsilon}$, where the scalar variable D describes the isotropic damage and $\mathbb{C}$ refers to the material tensor of the undamaged material. An evolution law and a damage surface are introduced. The damage surface $S(\epsilon^{\mathrm{eq}})$ distinguishes, whether damage develops or not. It depends on the equivalent strain ϵ^{eq}

$$\dot{D} = \Delta\lambda \frac{\partial S(\epsilon^{\mathrm{eq}})}{\partial \epsilon^{\mathrm{eq}}} \quad , \qquad S(\epsilon^{\mathrm{eq}}) = 1 - \exp\left[-\left(\frac{\epsilon^{\mathrm{eq}} - a}{\alpha}\right)^{\beta}\right] - D \leqslant 0 \quad . \tag{1}$$

For the visco-plastic model, a penalty formulation $\mathcal{P}$ is introduced, based on the second law of thermodynamics. The scalar variable η describes the viscosity and $\phi(f)$ denotes to the PENALTY-function. In order to describe different behavior in compression and tension, the DRUCKER-PRAGER yield surface is chosen.

$$\mathcal{P} = \boldsymbol{\sigma} : \dot{\boldsymbol{\epsilon}}^{\mathrm{pl}} + \tfrac{1}{\eta}\phi(f), \quad \phi(f) = \begin{cases} 0 & ; f \leq 0 \\ \frac{1}{m+1} f^{m+1} & ; f > 0 \end{cases}, \quad f = \alpha_f \mathrm{tr}\boldsymbol{\sigma} + \parallel \mathrm{dev}\boldsymbol{\sigma} \parallel - \sqrt{\tfrac{2}{3}} k_f \quad . \tag{2}$$

3 Homogenization

The effective material tensor $\mathbb{C}^{\text{eff}}$ maps the average of strain on the average of stress $\langle \boldsymbol{\sigma} \rangle := \mathbb{C}^{\text{eff}} : \langle \boldsymbol{\epsilon} \rangle$. Here, $\langle \bullet \rangle$ denotes the volume average within the RVE. With the finite-element solution, the stress and strain can be evaluated. Subsequently, the effective elastic material tensor $\mathbb{C}^{\text{eff}}$ is calculated through homogenization. A least-square approach is used to determine the effective material properties λ^{eff} and μ^{eff}

$$\begin{pmatrix} 2\text{tr}\langle \boldsymbol{\epsilon} \rangle \text{tr}\langle \boldsymbol{\sigma} \rangle \\ 4\langle \boldsymbol{\sigma} \rangle : \langle \boldsymbol{\epsilon} \rangle \end{pmatrix} = \begin{bmatrix} 6\text{tr}^2\langle \boldsymbol{\epsilon} \rangle & 4\text{tr}^2\langle \boldsymbol{\epsilon} \rangle \\ 4\text{tr}^2\langle \boldsymbol{\epsilon} \rangle & 8\langle \boldsymbol{\epsilon} \rangle : \langle \boldsymbol{\epsilon} \rangle \end{bmatrix} \cdot \begin{pmatrix} \lambda^{\text{eff}} \\ \mu^{\text{eff}} \end{pmatrix} \quad . \tag{3}$$

The interior geometry of the abovementioned RVE is statistically distributed. For a reliable analysis, the homogenization procedure is performed for a sufficient number of different RVEs. The probability density of the effective Young's-modulus E^{eff} and the effective Poisson's ratio ν^{eff} are shown in **Figure 4** and **5** for a set of 9200 RVEs. Both probability densities are GAUSSian like (dashed lines).

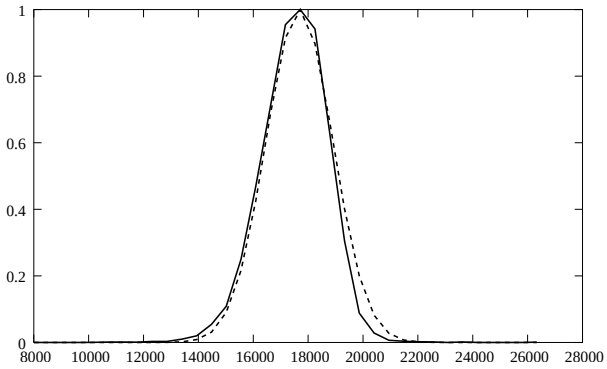

Figure 4: Probability density E^{eff}.

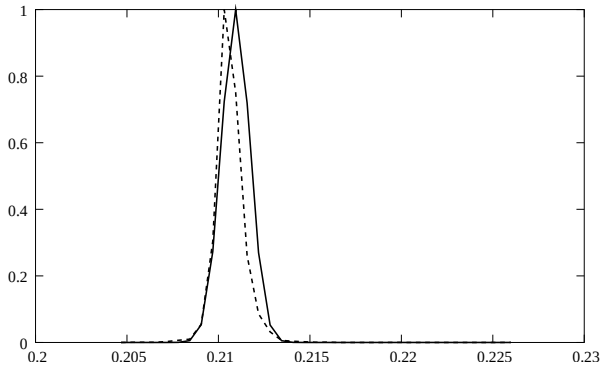

Figure 5: Probability density ν^{eff}.

The abovementioned numerical results fit with those obtained from experimental tests of hardened cement paste. The experimental tests are performed by the *Institut für Bauforschung* at the *RWTH Aachen*.

test	$E^{\text{eff}}_{\text{med}}\left[\frac{N}{mm^2}\right]$	$\nu^{\text{eff}}_{\text{med}}[-]$
numerical	17 665	0.211
experimental series 1	17 455	0.210
experimental series 2	17 727	0.210

Table 2: Experimental versus numerical results.

4 Parameter identification

The material model on the micro-scale contains inelastic parameters, which neither can be found in the literature, nor obtained through experimental testing. Therefor, one has to compute these by parameter identification. The identification is obtained by solving an optimization problem through a combination of the stochastic genetic algorithm and the deterministic LEVENBERG-MARQUARDT method. In a first step, a pre-optimization is performed with a genetic algorithm, in order to get close-to the global minimum. Once the value of the objective function falls below a certain threshold value, the optimization procedure switches to the more efficient LEVENBERG-MARQUARDT method.

In order to keep the overall computing time within reasonable bounds, the calculations are distributed within a network environment. A client-server based system was implemented to distribute these calculations automatically. A typical parameter identification requires approximately two month CPU time on a standard computer system. Within a network environment using 11 standard computers, the same identification was completed within 6 days, leading to a speed up of approximately 10.

Acknowledgment: Financial support from the *Deutsche Forschungsgemeinschaft* (German Research Foundation) DFG is gratefully appreciated.

REFERENCES

[1] Acker; Creep, Shrinkage and Durability Mechanics of Concrete and other Quasi-Brittle materials: proceedings of the sixth international conference **1** (2001); *Micromechanical analysis of creep and shrinkage mechanisms*; 15-25.

[2] Bernard, Ulm and Lemarchand; Cement and Concrete Research **33** (2003); *A multiscale micromechanics-hydration model for the early-age elastic properties of cement-based materials*; 1293-1309.

[3] Constantinides and Ulm; Cement and Concrete Research **34** (2004); *The effect of two types of CSH on the elasticity of cement-based materials: Results from nanoindentation and micromechanical modeling*; 67-80.

[4] Gross and Seelig; *Bruchmechanik* (Springer Verlag, 2001).

[5] Powers; Proceedings of the Fourth International Symposium on the Chemistry of Cement; Paper V-1 **2** Nr. 43 (1962); *Physical properties of cement paste*; 577-613.

[6] Powers and Brownyard; Research Laboratories of the Portland Cement Association Bulletin **22** (1948); *Studies of the physical properties of hardened portland cement paste*; 101-992.

[7] Zohdi and Wriggers; *An Introduction to Computational Micromechanics* (Springer Verlag, 2004).